Catalysis Communications 25 (2012) 78–82

Contents lists available at SciVerse ScienceDirect

Catalysis Communications

journal homepage: www.elsevier.com/locate/catcom

Short Communication

On the impact of Cu dispersion on CO_2 photoreduction over Cu/TiO_2

Dong Liu [a], Yolanda Fernández [a,b], Oluwafunmilola Ola [a], Sarah Mackintosh [a], Mercedes Maroto-Valer [a,*], Christopher M.A. Parlett [c], Adam F. Lee [c,*], Jeffrey C.S. Wu [d,*]

[a] Center for Innovation in Carbon Capture and Storage (CICCS), Faculty of Engineering, University of Nottingham, UK
[b] Instituto Nacional del Carbón, CSIC, Apartado 73, 33080, Oviedo, Spain
[c] Cardiff Catalysis Institute, School of Chemistry, Cardiff University, Cardiff CF10 3AT, UK
[d] Department of Chemical Engineering, National Taiwan University, Taipei, 10617, Taiwan

ARTICLE INFO

Article history:
Received 14 November 2011
Received in revised form 9 March 2012
Accepted 16 March 2012
Available online 27 March 2012

Keywords:
Photocatalysis
Titania
CO_2
Copper
Methane

ABSTRACT

A family of Cu/TiO_2 catalysts was prepared using a refined sol–gel method, and tested in the photocatalytic reduction of CO_2 by H_2O to CH_4 using a stirred batch, annular reactor. The resulting photoactivity was benchmarked against pure TiO_2 nanoparticles (synthesised by an identical sol–gel route). CO_2 photoreduction exhibited a strong volcano dependence on Cu loading, reflecting the transition from 2-dimensional CuOx nanostructures to 3-dimensional crystallites, with optimum CH_4 production observed for 0.03 wt.% Cu/TiO_2.

1. Introduction

The natural environment is well-versed in maintaining an equilibrium between carbon dioxide (CO_2) fixed through photosynthesis, and that released into the atmosphere via normal biochemical processes. However, this natural equilibrium has been strongly perturbed over the past few centuries through increased CO_2 emissions arising from fossil fuel combustion. The consequent dramatic rise in atmospheric CO_2 concentrations is well documented as the major contributor to ongoing climate change [1]. The most promising strategies proposed to slow, and eventually reverse, these rising CO_2 emissions are a switchover to renewable energy sources, or implementing carbon capture and storage

hence there exists great potential for new clean technologies for large-scale CO_2 fixation [3].

CO_2 photoreduction is one such promising method for ameliorating atmospheric CO_2 levels, while simultaneously providing energy-rich or chemically useful products such as CO, methane (CH_4), methanol (CH_3OH), formaldehyde (HCHO) or formic acid (HCOOH). A major challenge to such chemistry remains the development of efficient photocatalysts for direct CO_2 photoreduction offering high quantum yields, activity and selectivity. TiO_2 is widely used in photocatalysis due to it's low cost and toxicity, thermal stability and photo-response under UV irradiation, and thus may be viewed as a potential candidate for CO_2. However, the highest CO_2 photoreduction rate achieved using unpromoted TiO_2 is only 25 $\mu mol.g_{cat}^{-1}.hr^{-1}$ [4,5], and consequently too low for industrial commercialisation. Methods to modify the titania band gap, such as N-doping, or the addition of metal or oxide promoters to promote separation of photo-excited charge carriers and increase their lifetime for reaction with adsorbates, have both shown promise as routes to improve CO_2 photoreduction activity [6–8]. However, to date, there has been little effort to optimise promoter loadings or understand their impact upon TiO_2 catalysed CO_2 photoreduction. Here we systematically explore the influence of Cu promotion via incorporation during sol–gel synthesis, and demonstrate that n regulating the photo-y-dispersed (likely 2-dimensional islands) Cu_2O nanostructures maximise the CH_4 yield.

2. Experimental

2.1. Catalyst preparation

Pure and copper loaded TiO_2 were prepared by a modified sol–gel method adapted from Wu et al. [9] employing titanium (IV) n-butoxide ($Ti(OC_4H_9)_4$, Acros Organics, 99%) and copper (II) chloride ($CuCl_2.2H_2O$, Certified AR, 99%) precursors. To provide the stoichiometric amount of water for hydrolysis of the titanium precursor, 0.02 mol of $Ti(OC_4H_9)_4$ was mixed with 0.08 mol of n-butanol (C_4H_9OH, Certified AR, 99.5%) and 0.08 mol of acetic acid (CH_3COOH, Acros Organics, Glacial 99.8%).

* Corresponding authors. Tel.: +44 29208 74778; fax: +44 29208 74030.
E-mail address: leeaf@cardiff.ac.uk (A.F. Lee).

1566-7367 © 2012 Elsevier B.V. Open access under CC BY license.
doi:10.1016/j.catcom.2012.03.025

Cu-loaded TiO_2 was synthesised by pre-dissolving the desired amount of copper precursor (to provide 0.01–0.3 wt.% Cu/TiO_2) in the 0.08 mol n-butanol in order to achieve uniform copper incorporation throughout the titania support. Upon mixing the $Ti(OC_4H_9)_4$ with n-butanol and acetic acid, esterification of the latter two chemicals resulted in slow water release and $Ti(OC_4H_9)_4$ hydrolysis [10] which was complete after 6 h. The resulting sol–gel was placed in a chamber furnace and heated at 3 °C.min^{-1} to 150 °C and held for 2 h to dry the precursor. The temperature was then ramped at 5 °C.min^{-1} to 500 °C and held for 1 h to remove residual hydrocarbons and crystallise the titania. Samples were then ground by mortar and pestle for 20 min into powder form prior to CO_2 photoreduction tests.

2.2. Catalyst characterization

The resulting titanias were analysed by powder X-ray diffraction (XRD, Hiltonbrooks) to identify the associated crystal phases. Analyses were conducted using Cu K_α radiation at 1.5406 Å over $2\vartheta = 5°$–65° at 2°/min. Crystallite sizes were estimated from line broadening using the Scherrer equation [11]. Elemental analysis of the metal loaded TiO_2 catalysts was performed via ICP-MS (Thermo-Fisher Scientific X-series^{II}). The surface composition [12] and chemical environment was evaluated by X-ray photoelectron spectroscopy (XPS) on a Kratos AXIS HSi instrument using a Mg K_α excitation source and equipped with a charge neutraliser and magnetic focusing lens. Particle morphology was examined by transmission electron microscopy (TEM, JEOL 2100F, 200 kV) with analysis using a Gatan Orius camera and ImageJ 1.43u software. Total (BET) surface areas were determined by N_2 porosimetry using an ASAP 2020 instrument (Micromeritics); samples were dried at 80 °C and evacuated by vacuum overnight prior to analysis. Specific copper surface areas were determined by titration with N_2O [13], using a Quantachrome ChemBET™ TPR/TPD pulse-chemisorption system interfaced to an online MKS Minilab QMS. The following procedure was adopted: (i) 0.2 g of catalyst was outgassed at 110 °C for 30 min under He (20 ml.min^{-1}); (ii) the catalyst was then reduced at 280 °C for 30 min in flowing 10 vol.% H_2 in He (20 ml.min^{-1}); (iii) samples were cooled to 65 °C, and pure N_2O (Air Products) sequentially pulsed over the catalyst to react with metallic Cu and the resulting N_2O and N_2 pulses detected by mass spectrometry; (iv) complete titration was indicated by a constant N_2O peak area, consistent with oxidation of all Cu sites. The reductive pre-treatment temperature was selected following temperature-programmed reduction experiments, which showed that exposure to 10 vol.% H_2 at 280 °C was sufficient to fully reduce Cu in all our samples (Fig. S1), in accordance with previous literature on similar sol–gel Cu/TiO_2 materials [14]. A 1:2 N_2O:Cu stoichiometry was assumed in accordance with the literature, and the final Cu dispersion and specific surface area were calculated according to Eqs. (1) and (2):

$$\text{Cu dispersion}(\%) = \frac{\text{moles of Cu atoms on surface}}{\text{total moles of Cu atoms in sample}} \times 100 \quad (1)$$

$$\text{Cu surface area}\left(\text{m}^2\text{g}^{-1}\right) = \frac{\text{N} \times \text{C}}{\text{M}} \quad (2)$$

where N is the total number of surface Cu atoms, C is the cross section area of one Cu atom (6.803×10^{-20} m^2) and M is the bulk wt.% of the loaded Cu.

2.3. Photocatalytic testing

The photocatalytic reduction of CO_2 was conducted in a stirred batch annular quartz reactor with inner capacity of 316.9 ml. 200 ml of deionised water and 1 g of catalyst was added into this flat-bottomed quartz photo-reactor. A magnetic stirrer kept catalyst powders suspended throughout reactions. Ultra-pure gaseous CO_2 (Air Products, 99.995%) was then bubbled through the reactor for 20 min to degas the water. After purging, the reactor was pressurised with gaseous CO_2 at 1 bar, and held for 15 min to saturate the water with CO_2. The reactor was then isolated, and four 8-watt UVA (average intensity: 3.25 mW/cm^2, measured by UVX radiometer, UVP) lamps, located in two groups on opposing sides of the reactor, switched on to initiate photoreduction. Irradiation was stopped after 1.5-h reaction, and both gaseous and aqueous phase samples were injected into a gas chromatography equipped with a flame ionisation detector (GC/FID, Thermo-Fisher, Trace GC) to measure the concentration of the hydrocarbon product. Methane was the only organic product resulting from CO_2 photoreduction within the detection limits of our method (~200 ppb), although we cannot discount the possibility of CO formation which was undetectable on our GC. Methane yield was thus adopted as a direct measure of activity towards CO_2 photocatalytic reduction. Control experiments were regularly conducted to confirm methane arose solely from CO_2 photoreduction. The first control used pure He instead of CO_2; the second operated the reactor in a dark environment; and the final control omitted the photocatalyst. No products were observed in any of these controls.

3. Results and discussion

3.1. Catalyst characterization

Diffractograms of the pure and Cu-loaded titanias are shown in Fig. 1. Pure (pattern A) and Cu-loaded titania (patterns B–E) exhibited identical diffraction patterns to those of the anatase standard (Acros Organics, 99%, pattern F), with no additional reflections, indicating that only crystalline anatase was present in all materials. Crystallite sizes for pure and Cu loaded titania catalysts were calculated from peak broadening using the Scherrer equation, and indicated similar volume-averaged particle sizes of ~14 nm for all sol–gel prepared materials, significantly smaller than the commercial anatase (87 nm). Copper addition thus had negligible influence on the parent titania morphology or crystallinity.

Fig. 2 shows Cu 2p XP spectra of pure and selected Cu/TiO_2 catalysts (copper could not be detected at loadings below 0.5 wt.%). For the higher loading catalysts (≥0.5 wt.%) wherein copper was visible by XPS, the Cu $2p_{3/2}$ binding energy was constant at ~932.4 eV (indicative of Cu_2O [15]), with only the peak intensity rising with loading. While it is not possible to confirm the presence of surface copper (I) species at lower loadings, the independence of oxidation state on nominal loading between 0.5 and 2 wt.% Cu leads us to propose formation of a common Cu_2O species across our entire series. Surface and bulk copper compositions were quantified by XPS and ICP-MS respectively,

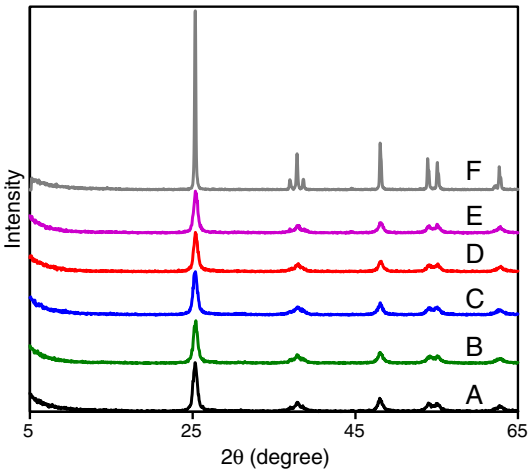

Fig. 1. XRD patterns of anatase standard, and pure and Cu loaded titania sol–gel catalysts: (A) Pure TiO_2; (B) 0.01 wt.% Cu/TiO_2; (C) 0.03 wt.% Cu/TiO_2; (D) 0.07 wt.% Cu/TiO_2; (E) 0.3 wt.% Cu/TiO_2; and (F) Anatase standard (Acros Organics, 99%).

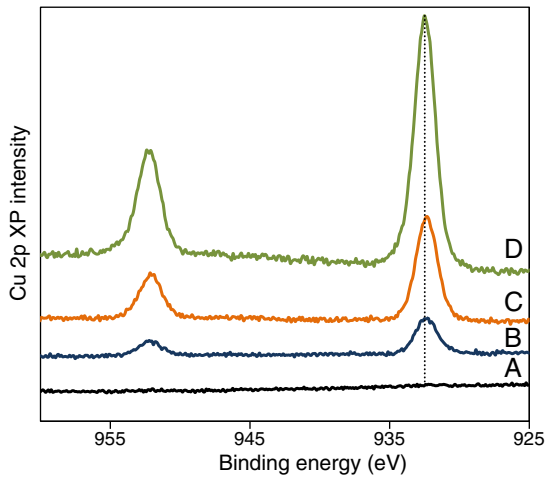

Fig. 2. Cu 2p XP spectra of: (A) Pure TiO_2; (B) 0.5 wt.% Cu/TiO_2; (C) 1 wt.% Cu/TiO_2; and (D) 2 wt.% Cu/TiO_2 sol–gel catalysts.

revealing significant Cu surface segregation with surface compositions of 1.2–8.7 wt.% versus bulk values spanning 0.47–1.76 wt.%, indicative of phase separated Cu_2O, rather than framework substituted Cu^+ ions.

Total surface areas of the commercial and sol–gel titanias are shown in Fig. S2 from which it is evident that Cu loading has little effect upon the textural properties of the sol–gel materials, with areas only decreasing by 10% from the parent TiO_2 across the series. It is interesting to note that the lowest (<0.02 wt.% Cu) loadings actually induce a small, but systematic *increase* in total surface area, before the subsequent net fall. Changes of this small magnitude are not expected to influence titania-related contributions to the resultant photoactivity [16,17], however, we believe these low loading surface area changes are a genuine effect associated with the formation of 2-dimensional Cu_2O islands. In contrast to the total areas, specific copper surface areas and associated dispersions are strongly loading dependent (Fig. 3). At loadings below 0.03 wt.%, Cu is essentially 100% dispersed, corresponding to either atomically isolated species, or 2-dimensional rafts (a partial encapsulating monolayer over the titania nanocrystallites). In the former scenario, the copper chemical environment should resemble that within a titanate, and not Cu_2O as observed by XPS, hence we can discount the presence of isolated Cu atoms. The initial plateau in dispersion for loadings up to 0.03 wt.%, followed by rapid fall towards zero for higher copper concentrations, strongly suggests the existence of two growth regimes: 2-dimensional Cu_2O island growth for loadings between 0.01 and 0.03 wt.%; and subsequent genesis and growth of 3-dimensional Cu_2O nanoparticles. This transition point occurs at very low effective Cu coverages, far below the nominal full monolayer, evidencing a Volmer–Weber growth mode, and poor wetting of titania by copper oxide as observed by STM [18] and XPS [19] over rutile TiO_2(110). Nucleation, growth and coalescence of oxide and metal nanoparticle on planar and porous substrates are complex processes [20–22], where we hope to utilise scanning probe microscopy and in-situ XAS to further investigate the atomic-scale structure of our Cu_2O nanostructures in the future.

3.2. Photocatalytic activity

CO_2 photoreduction was performed for 1.5 h during UVA irradiation and the resulting correspondence between methane yields and Cu dispersion/surface area is presented in Fig. 4. A strong volcano dependence of photoactivity for methane production with copper loading was observed for the sol–gel materials, wherein the CH_4 yield of the best-performing 0.03 wt.% Cu/TiO_2 catalyst was exhibited a 10-fold rate-enhancement over that of undoped titania. Since the mean TiO_2 crystallite sizes are all close to the optimal value (14 nm) for CO_2 photoreduction [23], and in common with their total surface areas, show little variance across the series, this pronounced effect cannot be attributed to geometric differences in the titania support. The extremely low copper concentrations necessary to achieve such promotion, with the maximum yield attained at only 400 ppm Cu, is especially striking, and also indicates a phenomenon arising from the promoter phase, rather than changes in the bulk properties of the titania parent. Fig. 4 demonstrates that CO_2 photoreduction is strongly associated with the exposed Cu_2O surface area; methane yield tailing off coincident with the switchover from 2-dimensional islands to 3-dimensional Cu_2O crystallites. It is interesting to note the different selectivity reported for higher loading Cu/TiO_2 photocatalysts prepared via a similar sol–gel route [6], wherein methanol and not methane was the primary product of CO_2 photoreduction. Although the origin of this copper loading dependence requires further investigation, it may reflect band gap broadening with Cu_2O crystallite size, affording more energetic photo-excited electrons necessary to drive the more thermodynamically difficult reduction of CO_2 to methanol ($E^o_{redox} = -0.38$ V vs. NHE, compared with −0.28 V for methane production) [4]. Peak methanol production reported in reference [6] (780 nmol/h/g) is also substantially higher than our best methane productivity (24 nmol/h/g), reflecting the widely disparate reaction conditions employed; specifically, the use of higher energy UVC in reference [6], which also utilised internal reactor illumination (resulting in a higher photon flux to the catalyst), and

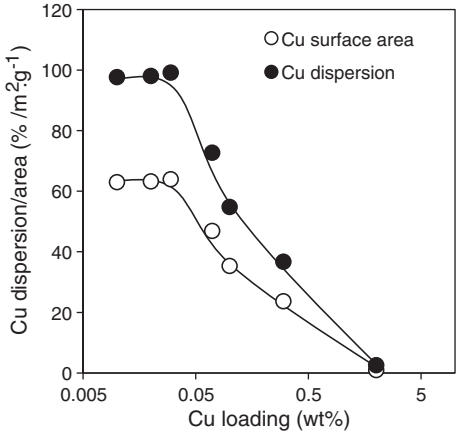

Fig. 3. Copper dispersion and specific surface area of Cu/TiO_2 sol–gel catalysts as a function of nominal bulk Cu loading.

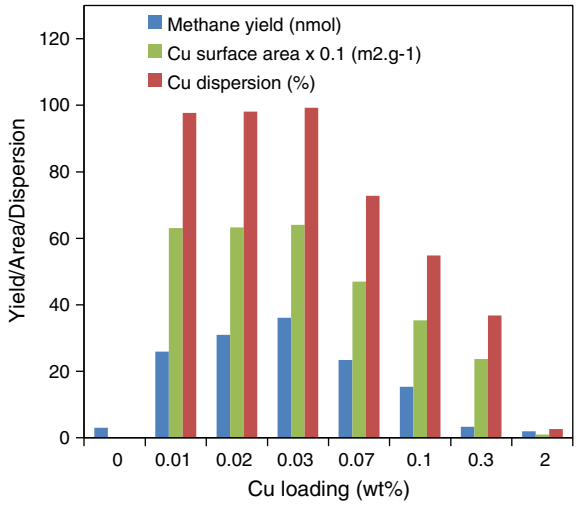

Fig. 4. Correspondence between 1.5 h CH_4 yield from CO_2 photoreduction over Cu/TiO_2 sol–gel catalysts and Cu surface area and dispersion.

crucially added NaOH to the reaction mixture to act as hole-scavengers suppressing recombination, all of which served to enhance methanol production.

3.3. Possible mechanism of copper promotion

It has been previously postulated that Cu^+ dopants (as free ions or the oxide) could serve as traps for photoexcited electrons or holes arising from TiO_2 [24,25]. Such electron–hole exchange could also occur between Cu_2O nanostructures and TiO_2 in this work, slowing slow e^-–h^+ recombination within the parent titania and thereby increasing the probability of electron transfer to adsorbed CO_2 and the genesis of reactive intermediates such as $\bullet CO_2^-$ and $HCOO^-$ [26–28]. Such charge-trapping is expected to be heavily influenced by the nature of the heterojunction interface between Cu_2O and TiO_2, with 2-dimensional copper oxide islands facilitating rapid charge migration from the underlying titania substrate (for subsequent CO_2 and water activation), while minimising the potential for bulk e^-–h^+ recombination within 3-dimensional Cu_2O crystallites [29,30]. If surface Cu_2O species are indeed the active centre for CO_2 photoreduction, then one would anticipate a linear correlation between photoactivity and Cu dispersion, precisely as seen in Fig. 5. It is important to recall that the band gap of Cu_2O lies in the visible, and thus may itself undergo direct photoexcitation upon UVA or solar irradiation, contributing to methane production. However, at the extremely low Cu concentrations found to be optimal within this study, it seems more probably that Cu_2O acts as an intermediary in CO_2 photoreduction, trapping and stabilising a high flux of photoexcited electrons created on titania, for transport to adsorbed carbon dioxide.

A recent in-situ DRIFTS study utilising isotopically-labelled $^{13}CO_2$ showed that surface carbon impurities may act as a carbon source for the production of reactively-formed hydrocarbons from CO_2 photocatalysis over titania, via the reverse Boudouard reaction, and corresponding intermediate CO formation [31]. Although Yui and co-workers have since used isotopic-labelling to unequivocally demonstrated that CO_2 can indeed be photoreduced to methane over TiO_2 and Pd/TiO_2 [32], the question remains as to what extent the reverse Boudouard reaction (4) competes with direct CO_2 photoreduction (3) as a source of methane, or indeed whether direct photo-oxidation of surface carbon may occur (5).

$$CO_2 + 2H_2O \rightarrow CH_4 + 2O_2 \quad \text{true photosynthesis via direct} CO_2 \text{ photoreduction} \quad (3)$$

$$CO_2 + C_a \rightarrow 2CO \quad \text{reverse Boudouard reaction (surface C participation)} \quad (4)$$

$$H_2O + C_a \rightarrow CO + H_2 \quad \text{photo-oxidation of surface carbon (no } CO_2 \text{ participation)} \quad (5)$$

The last scenario, namely whether methane arise from photo-oxidation of surface carbon by water (the only possible process by which it could form without direct participation of CO_2) can be easily discounted by a simple control experiment in which we exposed our catalysts to water and UV light in the absence of CO_2, resulting in negligible methane. This definitively proves that photo-activated CO_2 is an essential reactant in our methane production, as first postulated by Inoue and co-workers [33] and demonstrated by isotope-labelling experiments [31,34], enabling us to discount reaction (5). In order to assess the likely contribution of reaction (4), i.e. surface carbon assisted CO_2 photoreduction, to our observed methane yield, we examined the relationship between methane production and the initial surface carbon concentration of our as-prepared Cu/TiO_2 catalysts from XPS. Fig. 6 reveals a strong *inverse correlation* between carbon impurities on our as-prepared catalysts and methane production. While this does not conclusively prove that surface carbon plays no role in our observed photocatalysis, it offers strong evidence that the major route to reactively-formed methane is via direct CO_2 photoreduction and not carbon-assisted reverse disproportionation. It is important to note that the goal of this communication is not to elucidate the global reaction pathway in CO_2 photoreduction, but rather, to identify key structural aspects in Cu-doped TiO_2 photocatalysts to guide future materials design and thereby engineer improved methane production. Future isotope studies would be welcome to quantify the extent of any possible minor contributions from reaction (4).

4. Conclusions

Copper-loaded titania photocatalysts, prepared via a one-pot, sol–gel synthesis, comprise highly dispersed and surface localised Cu_2O nanostructures decorating 14 nm anatase crystallites. Cu_2O strongly promotes CO_2 photoreduction to methane under UVA light, with up to 10-fold rate-enhancements over the analogous unloaded anatase. This promotion is strongly linked to the nature of the dispersed copper oxide morphology, with 2-dimensional islands proposed both as trapping centres for anatase photoexcited charge carriers, and the primary active site responsible for CO_2 photoreduction. Formation of Cu_2O multilayers/nanoparticles at Cu loadings >0.03 wt.% limits the magnitude of this promotion, possible reflecting increased e^-–h^+ recombination within the bulk of 3-dimensional copper oxide crystallites. There is no evidence that reactively-formed methane arises from the reverse disproportionation reaction of CO_2 with surface carbon, although we cannot discount minor contributions from such a reverse Boudouard process.

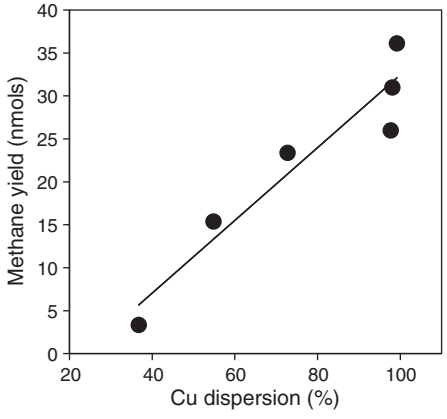

Fig. 5. Linear correlation between CH_4 yield and Cu dispersion over Cu/TiO_2 sol–gel catalysts.

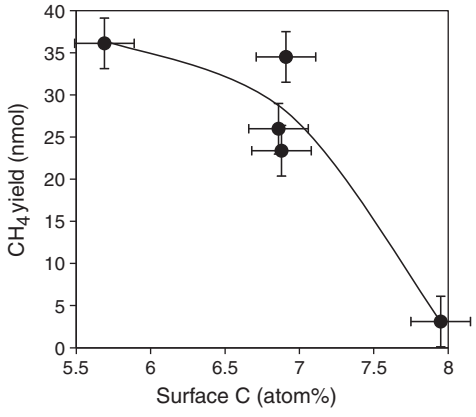

Fig. 6. Inverse correlation between 1.5 h CH_4 yield from CO_2 photoreduction over Cu/TiO_2 sol–gel catalysts and surface carbon content.

Acknowledgements

The authors acknowledge support from the Centre for Innovation in Carbon Capture and Storage (Engineering and Physical Sciences Research Council grant EP/F012098/1). This work was financially supported by the National Science Council under the project of NSC 98-2911-I-002-061 and The Royal Society International Project (JP090075). We thank Dr. Karen Wilson, Cardiff University, for XPS analysis. Y. Fernández is grateful to CSIC and FICYT of Spain for financial support under the Programme "Clarín" 2011–2012. AFL thanks the EPSRC (EP/G007594/2) for financial support and a Leadership Fellowship. MMV is grateful for support received through a Philip Leverhulme Prize.

Appendix A. Supplementary data

Supplementary data to this article can be found online at doi:10.1016/j.catcom.2012.03.025.

References

[1] D. Luthi, M. Le Floch, B. Bereiter, T. Blunier, J.M. Barnola, U. Siegenthaler, D. Raynaud, J. Jouzel, H. Fischer, K. Kawamura, T.F. Stocker, Nature 453 (2008) 379–382.
[2] F. Bowen, Energy Policy 39 (2011) 2256–2264.
[3] G. Centi, S. Perathoner, Catalysis Today 148 (2009) 191–205.
[4] V.P. Indrakanti, J.D. Kubicki, H.H. Schobert, Energy & Environmental Science (2009) 745–758.
[5] K. Ikeue, H. Yamashita, M. Anpo, T. Takewaki, The Journal of Physical Chemistry. B 105 (2001) 8350–8355.
[6] I.H. Tseng, W.C. Chang, J.C.S. Wu, Applied Catalysis B: Environmental 37 (2002) 37–48.
[7] Y. Li, W.N. Wang, Z. Zhan, M.H. Woo, C.Y. Wu, P. Biswas, Applied Catalysis B: Environmental 100 (2010) 386–392.
[8] H. Yamashita, H. Nishiguchi, N. Kamada, M. Anpo, Research on Chemical Intermediates 20 (1994) 823–825.
[9] J.C.S. Wu, I.H. Tseng, W.C. Chang, Journal of Nanoparticle Research 3 (2001) 113–118.
[10] J.C.S. Wu, Y. Yeh, Journal of Materials Research 16 (2001) 2-x.
[11] T. Lindgren, J.M. Mwabora, E. Avendano, J. Jonsson, A. Hoel, C. Granqvist, S. Lindquist, The Journal of Physical Chemistry. B 107 (2003) 5709–5716.
[12] B.G. Yacobi, Semiconductor materials: an introduction to basic principles, 7, Kluwer Academic/Plenum Publishers, New York, 2003, pp. 183–208.
[13] G.C. Chinchen, C.M. Hay, H.D. Vandervell, K.C. Waugh, Journal of Catalysis 103 (1987) 79–86.
[14] I.-H. Tseng, J.C.S. Wu, H.-Y. Chou, Journal of Catalysis 221 (2004) 432–440.
[15] Z.H. Gan, G.Q. Yu, B.K. Tay, C.M. Tan, Z.W. Zhao, Y.Q. Fu, Journal of Physics D 37 (2004) 81–85.
[16] Y. Jung, S.B. Park, Applied Catalysis B: Environmental 25 (2000) 249–256.
[17] G.H. Tian, H.G. Fu, L.Q. Jing, B.F. Xin, K. Pan, Journal of Physical Chemistry C 112 (2008) 3083–3089.
[18] J. Zhou, Y.C. Kang, D.A. Chen, The Journal of Physical Chemistry. B 107 (2003) 6664–6667.
[19] L. Huang, F. Peng, F.S. Ohuchi, Surface Science 603 (2009) 2825–2834.
[20] Chun-Ming Li, I.M. Robertson, M.L. Jenkins, J.L. Hutchison, R.C. Doole, Micron 36 (2005) 9–15.
[21] E.V. Zolotukhina, T.A. Kravchenko, Electrochimica Acta 56 (2011) 3597–3604.
[22] K. Højrup-Hansen, S. Ferrero, C.R. Henry, Applied Surface Science 226 (2004) 167–172.
[23] K. Koci, L. Obalova, L. Matejova, D. Placha, Z. Lacny, J. Jirkovsky, O. Solcova, Applied Catalysis B: Environmental 89 (2009) 494–502.
[24] M. Ni, M.K.H. Leung, D.Y.C. Leung, K. Sumathy, Renewable and Sustainable Energy Reviews 11 (2007) 401–425.
[25] M.I. Litter, Applied Catalysis B: Environmental 23 (1999) 89–114.
[26] H.J. Cardona, C. del Moral, C.R. Cabrera, Journal of Electroanalytical Chemistry 513 (2001) 45.
[27] O. Koga, T. Matsuo, N. Hoshi, Y. Hori, Electrochimica Acta 44 (1998) 903.
[28] Y. Hori, A. Murata, T. Tsukamoto, H. Wakebe, O. Koga, H. Yamazaki, Electrochimica Acta 39 (1994) 2495.
[29] Z. Zhang, C.C. Wang, R. Zakaria, J.Y. Ying, The Journal of Physical Chemistry. B 102 (1998) 10871–10878.
[30] W. Choi, A. Termin, M.R. Hoffmann, Journal of Physical Chemistry 98 (1994) 13669–13679.
[31] C.-C. Yang, Y.-H. Yu, B. van der Linden, J.C.S. Wu, G. Mul, Journal of the American Chemical Society 132 (2010) 8398–8406.
[32] T. Yui, A. Kan, C. Saitoh, K. Koike, T. Ibusuki, O. Ishitani, Applied Materials & Interfaces 3 (2011) 2594–2600.
[33] T. Inoue, A. Fujishima, S. Konishi, K. Honda, Nature 277 (1979) 637–638.
[34] N. Ulagappan, H. Frei, Journal of Physical Chemistry A 104 (2000) 7834–7839.